Computational fluid dynamics simulation of air flow in a spray dryer containing wall air pressure nozzle

Omid Reza Roustapour[1*], Mostafa Hosseinalipour[2], Hamid Reza Gazor[1]
Abolhasan Salehi[3]

(1. Agricultural Engineering Research Institute, Agricultural Research, Education and Extension Organization (AREEO), Karaj, Iran, 3135933151;
2. Iran University of Science and Technology, Tehran, Iran, 1684613114;
3. Graduated Student, Engineering College, Bafgh Branch, Islamic Azad University, Bafgh, Iran, 7189773757)

Abstract: Wall deposition is the main problem in a spray dryer that affects the quality of the powder and decreases the dryer operation. In the current study, the influence of using an air pressure nozzle on the conical section of the dryer chamber was examined by simulation of flow pattern in a pilot plant spray dryer using computational fluid dynamics (CFD) technique and Ansys Fluent software (Ver. 17.0). The governing equations are solved in an axisymmetric geometrical model meshed by quadratic elements. Flow pattern was studied and compared in two conditions: before and after considering air pressure nozzle in the dryer chamber wall. Verification of velocity magnitude revealed that there was a little difference (5% to 7%) between numerical and experimental values and there was a good correlation ($R^2 \geq$ 95%) between them. Flow pattern in the dryer chamber in absence of wall pressure nozzle showed recirculation zones were formed at the end of cylinder part of the chamber. Considering wall pressure nozzle in the model caused deflection of inflow towards the dryer wall and extension of chamber central core flow. The simulation results showed deviation of particle deposition from cone section towards the cylinder and ceiling parts of dryer.

Keywords: spray dryer, CFD, wall air pressure nozzle, flow pattern, particle deposition

Citation: Roustapour, O. R., M. Hosseinalipour, H. R. Gazor, A. Salehi. 2024. Computational fluid dynamics simulation of air flow in a spray dryer containing wall air pressure nozzle. Agricultural Engineering International: CIGR Journal, 26(3):134-147.

1 Introduction

One of the most important problems in a spray dryer is particle deposition in the dryer wall. In spray drying process, the most particles which do not succeed to get out from the dryer outlet, deposit on the cone part of the dryer chamber. The particles accumulate gradually during drying on the wall. This phenomenon cause to decrease the quality of particles because of thermal stress which receive during deposition on the wall for long period of time. The trajectory of particles and deposition of them have studied by many researchers. Kieviet (1997) assessed the particles trajectory and distribution in a spray dryer in order to manage deposition of particles.

Woo et al. (2008) investigated the condition of the amorphous particles impacting the wall of a spray dryer in order to clarify the deposition mechanism and involved physical phenomena in the drying chamber. They reported that the particles with high moisture content in contacting with a dryer wall,

Received date: 2023-04-11 **Accepted date:** 2024-04-03
[*]**Corresponding author: Omid Reza Roustapour,** Associate Prof., Agricultural Engineering Research Institute, Agricultural Research, Education and Extension Organization (AREEO), Karaj, Iran, postal code:313593315. Tel: +982636150000. Fax: +982632706277. Email: o.roostapour@areo.ir

containing particles with low moisture content, would deposit on the wall completely. Particles became rubbery at high temperature and liquid-bridge formed as the dominant deposition mechanism.

In another investigation, particle deposition on the wall was studied by utilizing computational fluid dynamics (CFD) method in a spray dryer and variation of surface energy on the chamber wall was measured. Results showed that the collection plates with lower surface energy (Teflon) obtained less deposition of amorphous particle comparing to stainless steel plates with higher surface energy. Stickiness of particles was controlled by temperature of process, effectively (Woo et al., 2009).

The multiphase flow in an industrial spray dryer was simulated by CFD method. The behavior of milk particles in the flow field during the drying process was analyzed. Results showed that the particle clouds whose sizes were between 224 and 285 μm, were generated near the conical side wall and transported upwards until they got separated from the straight side wall and dispersed into the air stream (Jin and Chen, 2009).

Air flow pattern in an industrial milk powder spray dryer was investigated. In absence of droplets, isothermal three-dimensional transient simulation was carried out applying the commercial CFD code (CFX10.0). The simulations showed the formation of a main air jet in the central axis and the recirculation zones between the main jet and the chamber walls. According to the results, there was a good adaptation between simulated absolute velocity period and the average telltale period (Gabites et al., 2010).

Low velocity flow in a pilot scale micro-fluidic spray dryer caused an increase residence time of particles in the dryer chamber. CFD simulation revealed that the effects of natural convection caused by heat loss from the wall, deflected air from the central core flow and spread it towards the wall. This phenomenon created recirculation regions in the center of the tower which influenced on the residence times particularly for the smaller particles. Results showed constricting the bottom outlet was an effective method for air-particle separation. This was due to the redirection of the air to escape from the side annulus outlet while the particles settled at the bottom (Woo et al., 2011).

Particle deposition was simulated in a spray dryer. Maltodextrin as a drying agent increased the glass transition temperature of Anthocyanin droplets and decreased their deposition on the wall (Patniboon et al., 2014).

Several factors such as wall temperature, dryer size and wall properties could have effect on particle deposition and energy loss. Studying particle trajectory and introducing suitable models to simulate behavior of spray drying by CFD method could optimize particle deposition (Keshani et al., 2015).

Strong swirling in a counter-current spray dryer caused to deposit particles in multi layers on the wall. Tracking the rate of release of particles from the walls permitted quantification of the age distribution of the re-entrained powder. Deposition rate of particles was between 12% and 20% of powder production which increased to 15% to 31% for particles smaller than 212 microns or 10% to 37% for particles larger than 850 microns (Francia et al., 2015).

The role of wall clustering in the operation of swirl spray dryers and the benefits of different control strategies based on manipulation of air temperature and velocity were investigated by CFD simulation (Francia et al., 2017). Results illustrated that air flow pattern affected size distribution of detergent powder and wall deposition. Particles gained kinetic energy of swirl which guided them toward the dryer wall and deposition occurred constantly.

CFD simulations of particle and droplet agglomeration in an industrial counter-current spray dryer were carried out under transient condition and a modified form of the stochastic collision agglomeration model was proposed. In order to verify the validity of performed simulation, particle size distribution of product powder calculated from the agglomeration model was compared with the particle size distribution of product obtained from the spray drying process. A good agreement of the simulation

result and calculations was observed (Jaskulski et al., 2018).

A steady-state mathematical model for a co-current spray dryer with a two- fluid nozzle was developed to improve particles production. The model includes mass, energy and momentum balances for both particulate and gaseous phases. Experimental data obtained in a Mini-Spray Dryer were used to validate the model. Droplet-size measurements were carried out by using laser diffraction. The effects of the nozzle operation condition such as droplet velocity and size distribution on the mean droplet size were analyzed. Results showed that porosity and droplet size distribution generated in the nozzle affected the fraction of respirable particles, fine recovery and particle deposition on dryer wall (Cotabarren et al., 2018).

Particle tracking through medium of a spray dryer was modeled by CFD method. Results depicted the self-sustainable flow fluctuations were intensified while the velocity of inlet air was increased. When flow field was considered as transient, particle residence was decreased in comparison with residence time of the particles in a simplified flow field fluctuation (Jubaer et al., 2020).

According to the results of numerical and experimental investigations being carried out by different researchers it can be deduced that wall deposition is a key processing problem in a spray dryer that indirectly affects the quality and quantity of the product. It is also revealed that the degree of wall deposition is influenced by several factors such as operating parameters, spray dryer design and wall properties.

Generally, in an industrial spray dryer, deposited particles are collected and guided toward the dryer outlet by air brooms which are assembled in the conical section of the dryer chamber. Particles deposit on the air broom gradually during spray drying process that cause the reduction of produced dried material. In the current research, the flow pattern in a pilot plant spray dryer was modeled by CFD method. The main goal of this study was to study the effect of utilizing air pressure nozzles on the flow field in conical section of the dryer chamber and its effect on reducing particles deposition.

2 Materials and methods

Flow in a pilot plant spray dryer with the volume of 5.6 m^3 was simulated by CFD. Diameter and height of the dryer chamber were 1.2 m and 2.83 m, respectively. The maximum feed rate in dryer was 6 kg h^{-1} and a two- fluid nozzle was used to convert liquid feed to droplets. Inflow was supplied by a main centrifugal fan with maximum air flow rate of 870 m^3 h^{-1}. The pilot plant spray dryer was design and manufacture by Fathi (2014) (Figure 1 a, b). Flow inside the spray dryer chamber was considered as axisymmetric and momentum and deposition of particles were determined.

(a) Image of the equipment (b) 3D dimensional structure

Figure 1 Pilot plant sprat dryer (Fathi, 2014)

2.1 Mesh generation and grid independency

The Gambit software (Ver. 17.0) (Anonymous, 2016) was applied to construct an axisymmetric model of the spray dryer. Air flow was led in the chamber through a circular distributor plate with 42 holes each of which was 25 mm in size and were arranged in three rows (Figure 2). Total area of holes (S_{TH}) was calculated from Equation 1 as 20616.7 mm^2. In order to simulate dryer as an axisymmetric model, air distributor plate was defined by three rows of annular ring with mean radiuses ($\bar{r}_i$) of 37.5 mm, 75 mm and 112.5 mm, respectively and thickness of *dr* (hydraulic diameter). Total area of rings (S_{TR}) was calculated from Equation 2 which is equal to total area of holes. By equivalent between two Equations 1 and 2, "*dr*" was obtained as 14.58 mm (Roustapour et al., 2009).

$$S_{TH} = \frac{n\pi d^2}{4} \quad (1)$$

$$S_{TR} = 2\pi dr \sum_{i=1}^{3} \bar{r}_i \quad (2)$$

Figure 2 The circular distributor plate of the spray dryer

Inlet air temperature, mass flow rate, turbulence intensity and hydraulic diameter of each air inlet ring should be considered in order to define the inflow boundary conditions as mass flow inlet. As long as the summation of residual mass flow rate value of total cells in a mesh is nearly equal to the inlet mass flow rate, the quality of solution convergence is acceptable. Accurate answers could be reached with minimum errors by a good selection of grid size. Comparison of the velocity magnitude, the turbulence kinetic energy (k) and the rate of dissipation (ε) for different meshes are necessary to reach an acceptable grid independency (Kieviet, 1997).

Quadratic elements with three different sizes were applied to mesh medium of dryer chamber. Suitable meshes were selected based on the least Y^+ (about 50) in wall boundaries. In order to reach grid independency, at least three types of meshes with different sizes of grid were produced. The number of cells in grid independency procedure was 53192, 57449 and 64560.

The problem was run in three defined meshes in Fluent Software (Ver. 17.0) (Anonymous, 2016) and velocity magnitude variation in two parts of the chamber including the middle of cylindrical part (40 cm distance from dryer ceiling) and the top of cone part (106 cm distance from dryer ceiling) were determined for three different mesh sizes and compared together to achieve grid independency (Figure 3 a, b).

In order to obtain the best mesh, variation of velocity among defined meshes should be less than 5% (Kieviet, 1997). For this purpose, the maximum values of velocity magnitude for three levels of mesh in two considered positions in the dryer chamber were obtained and the rate of variation between these values of velocity determined as Equation 3.

$$Rate\ of\ velocity\ \mathrm{var}iation\ (\%) = \frac{Difference\ between\ Max.velocity\ in\ two\ grids}{Max.velocity\ in\ the\ first\ comparison\ grid} \times 100 \quad (3)$$

The Maximum values of velocity magnitude for three levels of mesh in two distances from dryer ceiling are demonstrated in Table 1.

The rate of velocity variation between two mesh sizes of 53192 and 57449 cells in the middle of cylindrical part and the top of cone part of dryer were -4.08% and -0.073%, respectively. These values between two mesh sizes of 53192 and 64560 cells were -2.001% and +0.027% and between two mesh sizes of 57449 and 64560 cells were +2.17% and +0.1004%, sequentially. Based on the results, velocity variation between two mesh sizes of 57449 and 64650 cells was positive and less than 5% therefore, there was not any significant difference between two mentioned grids in two section areas of dryer and mesh sizes with 57449 cells was selected as

an optimized grid to solve problem. Figure 4 illustrates the optimized grid was produced in axisymmetric model.

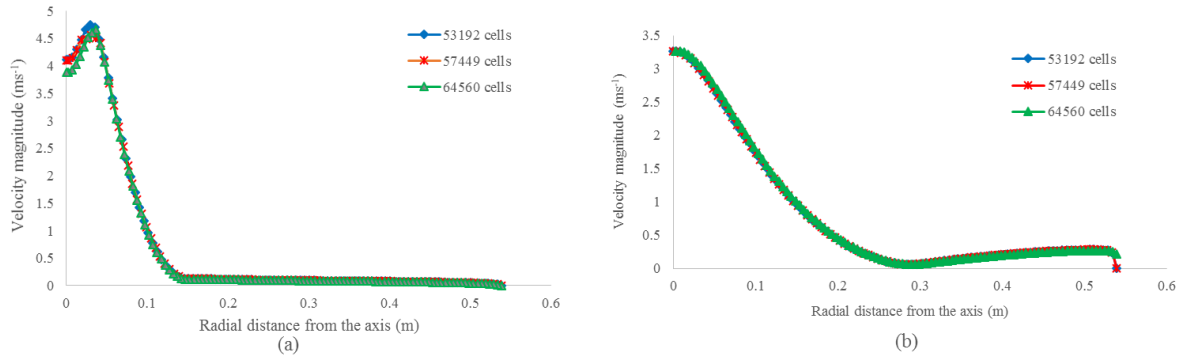

Figure 3 Comparison between variations of velocity magnitude for three levels of mesh; a) 40 cm from dryer ceiling, b) 106 cm from dryer ceiling

Table 1 The maximum values of velocity magnitude for three levels of mesh

Grid	Distance from dryer ceiling (cm)	Velocity magnitude in the axis (m s^{-1})
53192	40	4.75385
	106	3.26784
57449	40	4.55988
	106	3.26543
64560	40	4.65872
	106	3.26871

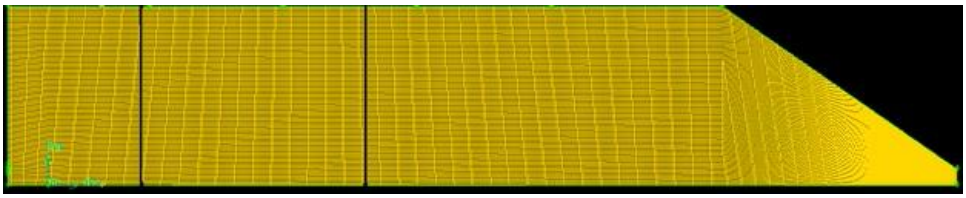

Figure 4 The mesh structure for the optimized grid with 57449 cells

An Eulerian– Lagrangian approach was used for two phase flow modeling. A one way coupling between the continuous and discrete phase was considered via appropriate mass, momentum and energy sources in the continuous phase governing equations. The interaction of droplets on the air flow inside the chamber was ignored because the mass ratio of droplets as a discrete phase to air as a continuous phase was very little.

2.2 Governing equations

The air conducted to the dryer chamber directly by a distributor plate without any spiral motion, therefore; inflow swirl angle was assumed zero in the simulations (Roustapour et al., 2009). The assumption a no-swirl axisymmetric flow in the spray dryer was made two-dimensional analyses valid.

The Navier-Stokes equations for an incompressible flow are as the followings:

$$\frac{\partial u}{\partial t}+(u.\nabla)u=-\frac{1}{\rho}\nabla P+\nu\nabla^2 u+g \quad (4)$$

Standard k– Ɛ model seems to be appropriate for internal flows with low swirl and turbulence intensity (Kieviet, 1997). This model is the most common model used to simulate mean flow characteristics for turbulent flow conditions (Oakley and Bahu, 1993):

$$\frac{\partial}{\partial t}(\rho k)+\frac{\partial}{\partial x_i}(\rho u_i k)=\frac{\partial}{\partial x_i}\frac{\mu_t}{\sigma_k}\frac{\partial k}{\partial x_i}+G_k-\rho\varepsilon \quad (5)$$

$$\frac{\partial}{\partial t}(\rho\varepsilon)+\frac{\partial}{\partial x_i}(\rho u_i \varepsilon)=\frac{\partial}{\partial x_i}\frac{\mu_t}{\sigma_\varepsilon}\frac{\partial \varepsilon}{\partial x_i}+C_{1\varepsilon}\frac{\varepsilon}{k}-C_{2\varepsilon}\rho\frac{\varepsilon^2}{k} \quad (6)$$

In which "*k*" is the turbulent kinetic energy and "$\mathcal{E}$" is the rate of dissipation of turbulent kinetic energy and C_μ, σ_k, σ_ε, $C_{1\varepsilon}$ and $C_{2\varepsilon}$ are empirical constant values as below (Versteeg and Malalasekera, 1995):

σ_k=1, σ_ε=1.3, $C_{1\varepsilon}$=1.44, $C_{2\varepsilon}$=1.92, C_μ=0.09

In accordance with inlet air velocity in dryer (13.15 m s^{-1}) and the speed of sound (340 m s^{-1}), the Mach number of turbulence was calculated by Equation 7 which was less than 0.3, so flow was

assumed as incompressible (Sarkar and Balakrishnan, 1990).

$$M = \frac{V}{a} \quad (7)$$

Implicit formulas were solved until the problem converged to accuracy of 10^{-10}.

2.3 Boundary conditions

As the flow was considered axisymmetric therefore the central axis of dryer was defined as "axis" boundary. Other boundaries such as inflow, outflow and total walls of the chamber were defined as "mass flow inlet", "pressure outlet" and "adiabatic wall with constant temperature", respectively. Wall temperatures were measured by several PT100 sensors. The temperature of dryer cylindrical and cone wall was 363 K averagely and the temperature of dryer ceiling wall was 409 K. Different experiments and measurements were conducted in the spray dryer in order to determine the boundary conditions including inlet air temperature, inflow, wall temperature, feed rate, air pressure of two fluid nozzle, dryer outlet temperature and properties of the air jet nozzle such as orifice hydraulic diameter, air flow rate and air pressure.

Total air inflow was 0.242 m^3 s^{-1} at inlet air temperature equaled to 136ºC. Air density at this temperature is 0.85333 kg m^{-3} (Incropera and Witt, 2002). Therefore, inlet mass flow rate was computed as 0.2 kg s^{-1}. In axisymmetric solution, the total mass flow divided by 2π, thus the final value of inflow was obtained as 0.032 kg s^{-1} in the model. The mass flow rate in any ring was determined based on their surface area of any ring and air velocities which were equal behind all rings. Turbulence intensity is necessary to define air inlet boundary condition as below (Anonymous, 2016):

$$\mathrm{Re}_{d_h} = \rho V d_h / \mu_a$$

$$I = u' / u_{ave} \cong 0.16(\mathrm{Re}_{d_h})^{-1/8} \quad (8)$$

The air conducted behind the air inlet rings by a circular channel with 153 mm in diameter. Inlet air velocity was determined as 13.15 m s^{-1} based on the air inflow of the main fan and section area of the dryer inflow channel. Turbulence intensity was calculated as 3.94% using Equation 8. Table 2 illustrates the inlet air properties with an initial temperature of 136ºC and boundary conditions of inlet channel (Incropera and Witt, 2002).

Table 2 Initial conditions of air inlet channel

Turbulence intensity (I) (%)	Reynolds number (Re_{dH})	Viscosity (μ) (kg m^{-1} s^{-1})	Hydraulic diameter (d_H) (m)	Air inlet velocity (V) (m s^{-1})	Air density (ρ) (kg m^{-3})
3.94	73938	2.322×10^{-5}	0.153	13.15	0.85333

Air velocity magnitude, turbulence intensity and hydraulic orifice diameter of air pressure nozzle should be determined in order to define 4 air pressure nozzles with orifice diameter of 1 mm in the junction of cylinder and cone sections of the dryer chamber. Air was supplied to the nozzles with a volumetric rate of 2.25 m^3 h^{-1} and pressure of 3.5 bar by a compressor. Air flow rate was determined by a rotameter and air pressure was adjusted by a regulator. In order to solve the problem as an axisymmetric medium, nozzles defined as a ring with hydraulic diameters equaled to 8.33×10^{-4} mm (Equation 2). In this condition, air velocity in the ring was determined as 31.7 m s^{-1}. The Mach number of the air pressure nozzle was calculated as 0.1 which was less than 0.3; therefore, the air flow was assumed as incompressible in the nozzle. Reynolds number and turbulence intensity were computed by Equation 8. Table 3 illustrates the flow specification and boundary conditions of air pressure nozzle.

Table 3 Boundary conditions for air pressure nozzle

Turbulence intensity (I) (%)	Reynolds number (Re_{dH})	Viscosity (μ) (kg m^{-1} s^{-1})	Hydraulic diameter (d_H) (mm)	Air pressure velocity (V) (m s^{-1})	Air density (ρ) (kg m^{-3})
4.08	55840	1.789×10^{-5}	0.00083	31.7	1.255

Boundary conditions were depicted in Figure 5 schematically. Variation of velocity magnitude was studied in two vertical positions of dryer tower including 40 cm distance from dryer ceiling in

cylindrical part and 106 cm distance from dryer ceiling near the junction of cylinder and cone parts of the dryer chamber.

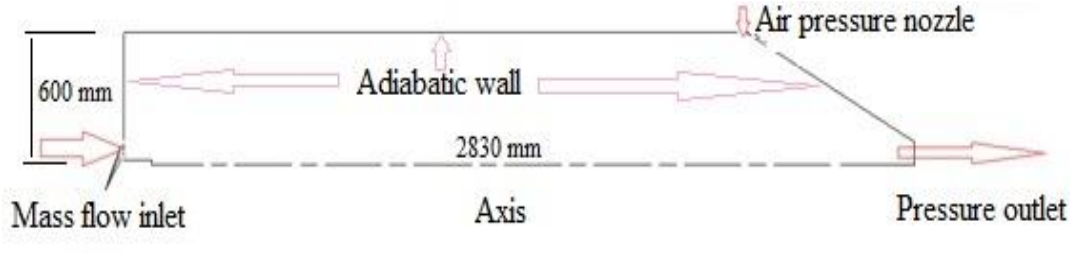

Figure 5 Axisymmetric model of spray dryer and boundary conditions

2.4 Model validation

In order to confirm simulation results, velocity variation was measured in two sections of the dryer by a hot wire anemometer, AM20 model of Lutron Company, Taiwan and compared with velocity magnitude pattern of the model. Goodness of fit validated by applying a statistical criterion as coefficient of determination (R^2), Equation 9. It was calculated using Minitab software (version 15, Minitab Inc. USA). The coefficient of determination (R^2) value near to 1 was better for goodness of fit (Yaldýz and Ertekýn, 2001). This parameter has been calculated as follows (Madamba et al., 1996):

$$R^2 = \left[1 - \frac{\sum_{i=1}^{N}(MR_{\exp,i} - MR_{Model,i})^2}{\sum_{i=1}^{N}(MR_{\exp,i})^2}\right] \times 100 \quad (9)$$

2.5 Particle size distribution modeling

Particle size distribution was simulated based on random tracking method. Trajectory of particles was estimated via stochastic tracking in flow field and solving their equations (Anonymous, 2016).

Particle size distribution depends on their Reynolds number and gravity force on them, so residence time is related to momentum of particles and air flow pattern in the dryer (Huang et al., 2005).

Initial conditions of droplets as discrete phase were considered same as Sayyari et al. (2010) in order to determine particle distribution and their deposition on the dryer wall. Therefore, three groups of particle size containing 17, 77 and 137 microns were defined and 25 replications of tracking were considered estimating particle trajectory by stochastic modeling. The Rosin- Rammler method was applied to simulate the particle size distribution during flying in dryer air flow as a discrete phase. Finally, the numbers of particles which deposited on wall boundaries or exited from the outlet were estimated in simulation process.

3 Results and discussion

Air flow pattern affected particles trajectory and their collision with wall boundaries of the dryer chamber. It was distinguished by Francia et al. (2017). Results depict that variation of velocity is related to inlet air velocity, turbulence intensity and velocity vector direction.

3.1 Velocity vector and stream line before applying air pressure nozzle in the chamber

Figures 6 and 7 demonstrate velocity vector and stream line of flow in absence of air pressure nozzle on wall of the chamber. In accordance with the results, the flow field was made up of a high velocity core flow zone and a recirculation zone around the core. The core flow was extended toward the chamber outlet and led flow stream toward the cone wall or outlet of dryer. Vortex flow was formed near the junction of cylindrical and conical sections of the chamber. Then, these vortices extended up in the chamber around the core flow. It was similar to the results presented by Huang and Mujumdar (2007). In this flow, velocity vector depicted velocity variation nearly ranging from 7 m s^{-1} to 1 m s^{-1}.

3.2 Velocity vector and stream line with air pressure nozzle in the chamber

Results showed that using an air pressure nozzle on the dryer wall decreased particles deposition on the cone wall of the dryer chamber.

Figures 8 and 9 depict velocity vector and stream line of flow in the chamber containing air pressure nozzle on the wall. As soon as the air entered the chamber, it deviated to the cylindrical wall and generated vortex flow. The core flow extended up in the chamber and formed vortices around the core extended toward the outlet. Air at the junction of cylindrical and conical sections guided toward the outlet due to the vacuum created by wall air pressure nozzle. This phenomenon reduced particle deposition on the cone wall. The acquired air flow pattern was alike the attained flow pattern by Southwell et al. (1999). In this flow, velocity vector depicted velocity variation nearly ranging from 35 (In top of the cylinder part, bellow the nozzle) to 260 m s^{-1} (near the junction of cylinder and cone part of the chamber).

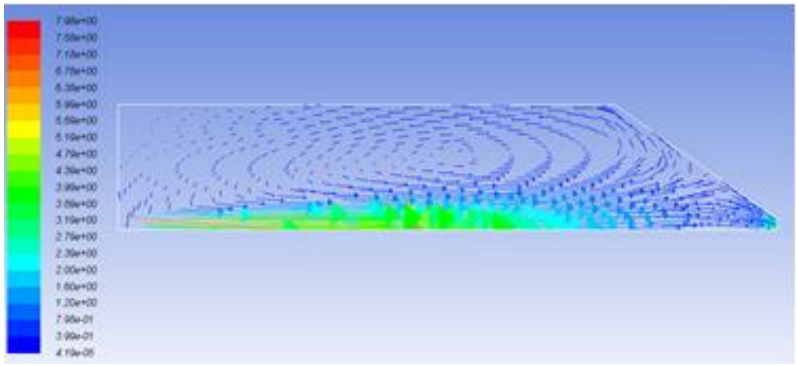

Figure 6 Velocity vectors in the dryer chamber in absence of wall pressure nozzle

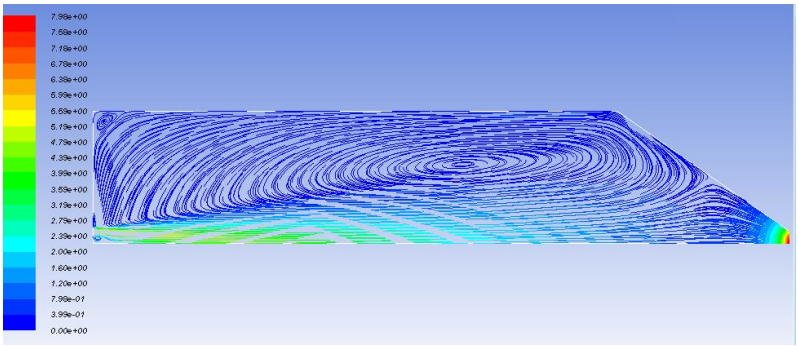

Figure 7 Flow stream line in the dryer chamber in absence of wall pressure nozzle

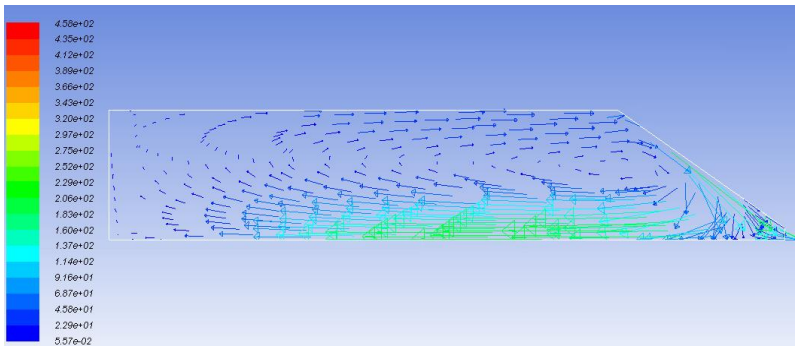

Figure 8 Velocity vectors in the dryer chamber with wall pressure nozzle

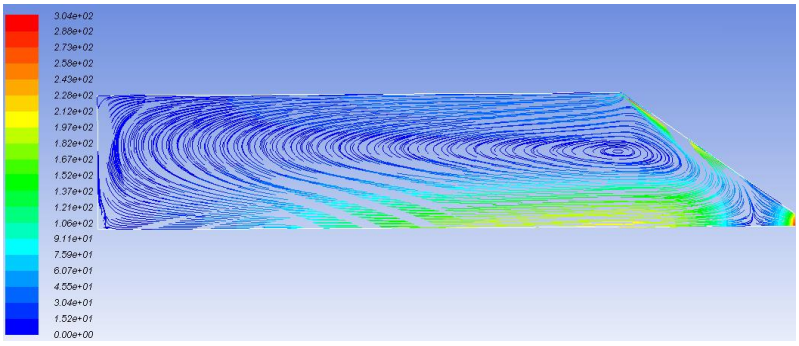

Figure 9 Flow stream line in the dryer chamber with wall pressure nozzle

3.3 Radial variation of velocity magnitude in absence of wall air pressure nozzle

Radial variation of velocity magnitude in absent definition of air pressure nozzle is demonstrated in two vertical distances which are 40 cm and 106 cm from the ceiling of the dryer chamber (Figure 10). In cylindrical part (40 cm height from the dryer ceiling), maximum velocity was observed in central core of flow. Near the junction of cylinder and cone parts of the chamber (106 cm height from the dryer ceiling), the effect of inflow was decreased, so velocity variation was more uniform here. To get further distance radially from the core flow, velocity magnitude reduced gradually so that velocity approached to zero across the chamber wall. In cone part, velocity magnitude had more value than that in the upper zone of the chamber.

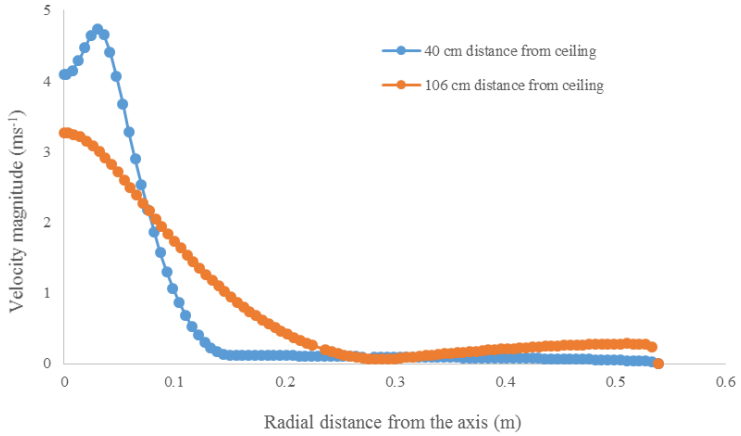

Figure 10 Radial variation of velocity magnitude in two altitudes from dryer ceiling- In absence of air pressure nozzle

According to the obtained results by Huang et al. (2005) which simulated velocity variation in a short form spray dryer with a rotary atomizer, vortices near the cone part of dryer were the cause of increase in velocity magnitude.

3.4 Radial variation of velocity magnitude with wall air pressure nozzle

Radial variation of velocity magnitude after placing air pressure nozzle is illustrated in two vertical distances that are 40 and 106 cm from the ceiling of the dryer chamber (Figure 11). It was concluded that utilizing air pressure nozzle increased velocity in the chamber. Velocity magnitude in cone part was by far much more than the upper part of the dryer chamber because the air pressure nozzle caused a great increase in velocity in installation zone. Results distinguished that velocity magnitude had the maximum value in central core flow. It could be observed that the velocity was increased near the outlet wall boundary. It happened due to the reduction of the hydraulic diameter here (Huang and Mujumdar, 2007).

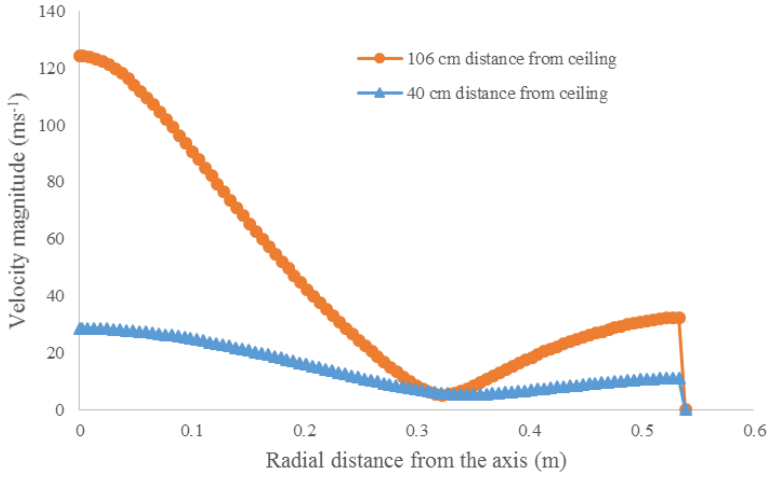

Figure 11 Radial variation of velocity magnitude in two altitudes from dryer ceiling- with air pressure nozzle

3.5 Simulation verification

Figure 12 demonstrates air velocity confirmation in cross section area of the chamber in two altitudes; 40 cm and 106 cm from the dryer ceiling. Generally, numerical and empirical results revealed a deviation of 5% to 7%. Based on the simulation results, velocity magnitude was zero on the wall boundary. When hot wire anemometer was used to measure velocity, definitely it could only record velocity data near the boundary layer of wall in vortices region. Therefore, a little difference between simulation and measured velocity data was expected.

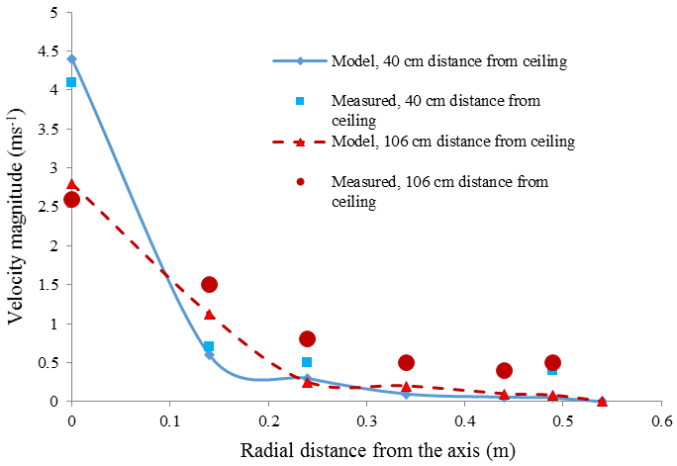

Figure 12 Radial velocity verification in two altitudes from dryer ceiling

A comparison between model and measured values of velocity variation in two sections of dryer chamber displayed a good correlation ($R^2 \geq$ 95%) among these values through linear equations (Figure 13 a, b) (Asadi et al., 2012).

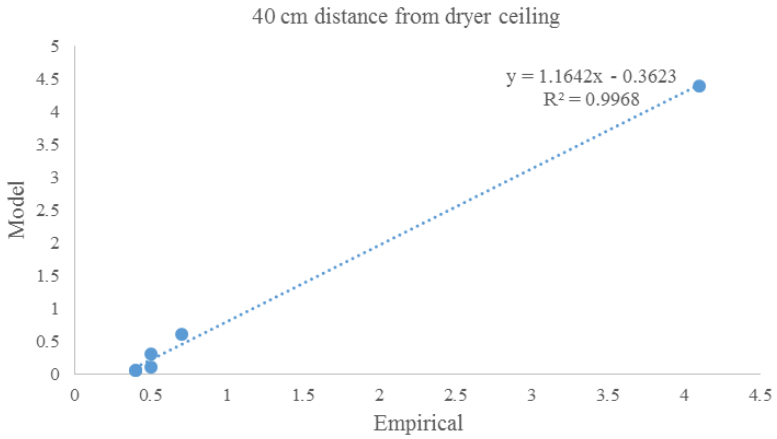

(a) 40 cm from dryer ceiling

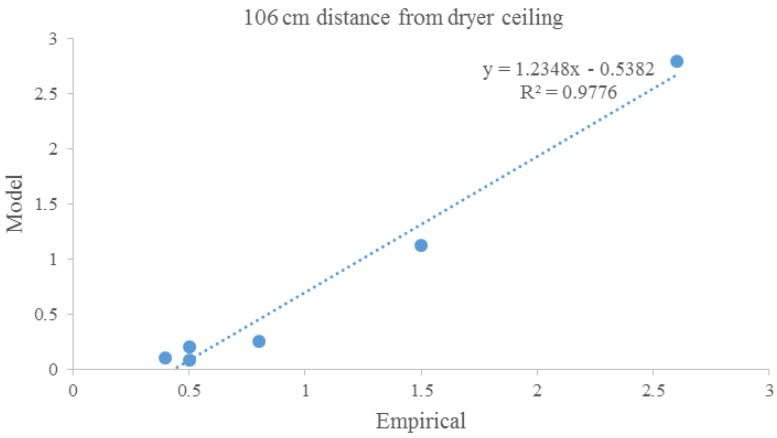

(b) 106 cm from dryer ceiling

Figure 13 Comparison between model and empirical velocity values in two sections of dryer tower

3.6 Particle deposition in two conditions: In absence of air pressure nozzle/With air pressure nozzle

Figure 14 (a, b) illustrates particle distribution in the dryer chamber with air pressure nozzle or in absence of that in the junction of cylinder and cone sections of the dryer chamber. Results displayed air flow of pressure nozzle on the cone wall caused to decrease deposition of particles here.

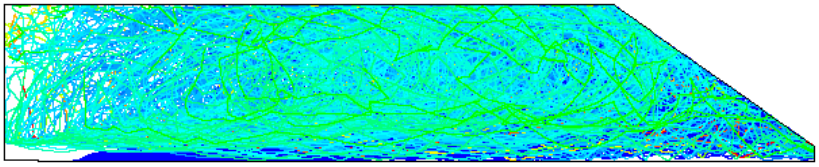

(a) In absence of air pressure nozzle

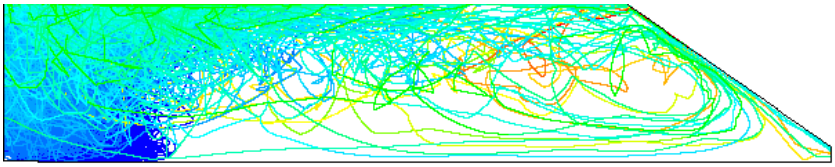

b) With air pressure nozzle

Figure 14 Particles distribution in the dryer chamber

Table 4 represents a fraction of deposition of different particles size groups on cylinder part, cone part, ceiling and outlet of the dryer chamber either with air pressure nozzle or in absence of that. It was revealed that deposition is related to particle size.

Table 4 Particle deposition on dryer wall and outlet either in presence or in absence of air pressure nozzle (%)

Droplets diameter (μm)		Cone part	Cylindrical part	Dryer outlet	Dryer ceiling
17	Particle deposition percent-Absence of air pressure nozzle	31	51	17	2
77		67	24	9	0
137		85	1	13	0
17	Particle deposition percent-With air pressure nozzle	0.5	57	10	33
77		0	37	0.1	63
137		0.1	34	0.1	62

Figure 15 The effect of using air pressure nozzle to broom particles on the cone wall

After considering wall air pressure nozzle, particles groups with diameter of 77 μm and 137 μm had the most deposition on the cone part of the chamber while particles with mean diameter of 17 μm had the most deposition on cylinder part of the chamber (Sayyari et al., 2010). In the chamber with wall air pressure nozzle, deposition of all particle size groups on cone part of the chamber decreased significantly. On the other hand, deposition on the ceiling and cylinder part of the chamber increased. Finally, particles which deviated toward the top of the dryer chamber, returned to the dryer outlet by vortices that were generated around the central core flow. Using air pressure nozzle in the cone wall caused to deviate more fractions of particles toward the outlet and decrease particle deposition on the dryer wall,

therefore it could be expected an increase in the dryer yield. Figure 15 shows the effect of installation the air pressure nozzle in the cone wall. The nozzle caused to sweep particles and prevented of particle deposition on the cone wall of dryer.

4 Conclusion

Air flow in the dryer chamber with wall air pressure nozzle and in absence of that was simulated and compared together and the results can be drawn as follow:

Air flow pattern in the dryer chamber in absence of air pressure nozzle on the dryer wall showed recirculation vortices were formed near top of the junction between cylinder part and cone part of the chamber. These vortices extended up in the medium and joined at the central core flow and were led to the outlet finally, but when air pressure nozzle was considered in the model, inflow was deviated toward the dryer chamber wall instantaneously.

Air flow in central core flow with wall air pressure nozzle, had maximum value around the junction of cylinder part and cone part and extended up in the chamber.

High velocity air pressure nozzle created a recirculation flow around the central core which conducted flow toward the outlet. When air pressure nozzle was not spotted, velocity magnitude of air flow was decreased gradually during recirculating toward the dryer outlet from 7 m s^{-1} to 1 m s^{-1}. Air velocity had the maximum value in central core flow and was reduced as deviated toward the dryer wall. But after defining wall air pressure nozzle, velocity magnitude had maximum value near the junction of cylinder part and cone part (about 260 m s^{-1}) in comparison with the top region of the chamber (about 35 m s^{-1}).

Verification results showed velocity variation in the model had maximum differences between 5 to 7 percent from empirical data. Although turbulence flow caused an increase in deviation between simulation and measured data in some region of the chamber. Comparison between model and measured values of velocity variation displayed a good correlation between these values through linear equations.

When air pressure nozzle was considered in the chamber, particle deposition in cone part decreased more than 95% and deviated toward cylinder part and ceiling of the dryer. It should be noted that particles continued their path toward the dryer outlet eventually.

References

Anonymous. 2016. ANSYS FLUENT 17.0 User's Guide. XX: Fluent Inc.

Asadi, V**.**, M**.** H**.** Raoufat, and S**.** M. Nassiri. 2012. Fresh egg mass estimation using machine vision technique. *International Agrophysics*, 26: 229-234.

Cotabarren, I. M., D. Bertín, M. Razuc, M. V. Ramírez-Rigo, and J. Piña. 2018. Modeling of the spray drying process for particle design. *Chemical Engineering Research and Design*, 132: 1091-1104.

Fathi, D. E. 2014. Design, development and evaluation of a pilot plant spray dryer with a two fluid nozzle in order to produce tomato Juice powder. M.S. thesis, Islamic Azad University, Eghlid Branch, Iran.

Francia, V., L. Martín, A. E. Bayly, and M. J. H. Simmons. 2015. Deposition and wear of deposits in swirl spray dryers: The equilibrium exchange rate and the wall-borne residence time. *Procedia Engineering*, 102: 831-840.

Francia, V., L. Martín, A. E. Bayly, and M. J. K. Simmons. 2017. Agglomeration during spray drying: Airborne clusters or breakage at the walls? *Chemical Engineering Science*, 162: 284-299.

Gabites, J. R., J. Abrahamson, and J. A. Winchester. 2010. Air flow patterns in an industrial milk powder spray dryer. *Chemical Engineering Research and Design*, 88(7): 899-910.

Huang, L., M. L. Passos, K. Kumar, and A. S. Mujumdar. 2005. A three-dimensional simulation of a spray dryer fitted with a rotary atomizer. *Drying Technology*, 23(9-11): 1859-1873.

Huang, L., and A. S. Mujumdar. 2007. Simulation of an industrial spray dryer and prediction of off- design performance. *Drying Technology*, 25(4): 703-714.

Incropera, F. P., and D. P. De Witt. 2002. *Introduction to Heat Transfer*. 4th ed. New York, USA: John Wiley & Sons.

Jaskulski, M., P. Wawrzyniak, and I. Zbiciński. 2018. CFD

simulations of droplet and particle agglomeration in an industrial counter-current spray dryer. *Advanced Powder Technology*, 29(7): 1724- 1733.

Jin, Y., and X. Chen. 2009. Numerical study of the drying process of different sized particles in an industrial scale spray dryer. *Drying Technology*, 27(3): 371-381.

Jubaer, H., S. Afshar, G. L. Maout, S. Mejean, C. Selomulya, J. Xiao, X. Chen, R. Jeantet, and M. W. Woo. 2020. The impact of self-sustained oscillations on particle residence time in a commercial scale spray dryer. *Powder Technology*, 360: 1177-1191.

Keshani, S., W. R. W. Daud, M. M. Nourouzi, F. Namvar, and M. Ghasemi. 2015. Spray drying: An overview on wall deposition, process and modeling. *Journal of Food Engineering*, 146: 152-162.

Kieviet, F. G. 1997. Modeling quality in spray drying. Ph.D. diss., Endinhoven University of Technology, the Netherlands.

Madamba, P. S., R. H. Driscoll, and K. A. Buckle. 1996. The thin layer drying characteristics of garlic slices. *Journal of Food Process Engineering*, 29(1): 75-97.

Oakley, D. E. and R. E. Bahu. 1993. Computational modelling of spray dryers. *Computational and Chemical Engineering*, 17(1): 493-498.

Patniboon, A., P. Ponpesh, A. Soottitantawat, and A. Arpornwichanop. 2014. Theoretical analysis of the wall deposition of particles in spray dryers. *Chemical Engineering Transactions*, 39: 571-576.

Roustapour, O. R., M. Hosseinalipour, B. Ghobadian, F. Mohaghegh, and N. M. Azad. 2009. Proposed a numerical–experimental method for drying kinetics in a spray dryer. *Journal of Food Engineering*, 90(1): 20-26.

Sarkar, S., and L. Balakrishnan. 1990. Application of a Reynolds-Stress turbulence model to the compressible shear layer. ICASE Report, No. 90- 18, NASA Contractor Report 182002.

Sayyari, A. R., O. R. Roustapour, A. R. Tahhavor, and A. Afsari. 2010. Numerical simulation of particle trajectories and velocity in a pilot plant spray dryer with a two-fluid nozzle. In *17th International Drying Symposium (IDS 2010)*, 387-391. Magdeburg, Germany, 3-6 Oct. 2010

Southwell, D. B., T. A. G. Langrish, and D. F. Fletcher. 1999. Process intensification in spray dryers by turbulence enhancement. *Chemical Engineering Research and Design*, 77(3): 189-205.

Versteeg, H. K., and W. Malalasekera. 1995. An introduction to computational fluid dynamics. In *Fluid Flow Handbook*, eds. N. Ashgriz, and J. Mostaghimi, ch. 20, 1-52. Longman, Malaysia: TCP.

Woo, M. W., W. R. W. Daud, S. M. Tasirin, and M. Z. M. Talib. 2008. Amorphous particle deposition and product quality under different conditions in a spray dryer. *Particuology*, 6(4): 265-270.

Woo, M. W., W. R. W. Daud, S. M. Tasirin, and M. Z. M. Talib. 2009. Controlling food powder deposition in spray dryers: Wall surface energy manipulation as an alternative. *Journal of Food Engineerin*g, 94(2): 192-198.

Woo, M. W., S. Rogers, S. X. Q. Lin, C. Selomulya, and X. Chen. 2011. Numerical probing of a low velocity concurrent pilot scale spray drying tower for mono-disperse particle production- unusual characteristics and possible improvements. *Chemical Engineering and Processing: Process Intensification*, 50(4): 417-427.

Yaldýz, O., and C. Ertekýn. 2001. Thin layer solar drying of some vegetables. *Drying Technology*, 19(3): 583-596.

Nomenclature

a	Speed of sound, m s^{-1}
d	Holes diameter of air inlet plate, *mm*
dr	Thickness of annular ring (hydraulic diameter), *mm*
g	Gravity, m s^{-2}
$\overline{h}$	Heat transfer coefficient, $Wm^{-2}K^{-1}$
I	Turbulence intensity
k	Turbulence kinetic energy, $m^2\ s^{-2}$
L	Height of cylinder and cone parts, *m*
MR_{exp}	Experimental moisture ratio
MR_{model}	Modeling moisture ratio
M_T	Mach number of turbulence
n	Number of air inlet holes
N	Number of observations
$\overline{Nu}_L$	Nusselt number
R^2	Coefficient of determination
$\overline{r}_i$	Mean radius of every air inlet ring
Re_{dh}	Reynolds number
S_{TH}	Total inlet air holes area, mm^2
S_{TR}	Total rings area, mm^2
u	The flow velocity, $m\ s^{-1}$
u'	The velocity fluctuations, $m\ s^{-1}$
u_{ave}	The mean flow velocity, $m\ s^{-1}$
V	Inlet air velocity, $m\ s^{-1}$
ε	Turbulence dissipation rate, $m^2\ s^{-3}$
μ_a	Air dynamic viscosity, $kgm^{-1}s^{-1}$
μt	Turbulence viscosity, $kgm^{-1}s^{-1}$
ρ	Fluid density, kgm^{-3}
θ	Thermal conductivity coefficient, $Wm_{-1}K^{-1}$
∇_p	Pressure gradient, Pa